كلية الهندسة بشبرا
FACULTY OF ENGINEERING AT SHOUBRA
ERJ
PRINT ISSN 3009-6049
ONLINE ISSN 3009-6022

ENGINEERING RESEARCH JOURNAL (ERJ)
Volume (53) Issue (4)
October. 2024, pp:137-145
https://erjsh.journals.ekb.eg

Experimental and Numerical Evaluation of Thin Concrete Slabs Reinforced with Textile Carbon Fiber

Hossam Mohy Ellaban*[1], Tarek S. Mustafa[1], Mossad Ali[1] , Tarek Abdelgalil[1]

[1]Department of Civil Engineering, Faculty of Engineering at Shoubra, Benha University, Cairo, Egypt.
* Corresponding Author.
E-mail: hossam.mohy@feng.bu.edu.eg, tarek.mohamed@feng.bu.edu.eg, mosaad.ali@feng.bu.edu.eg, tarek.abdelgalil@feng.bu.edu.eg

Abstract: This study explores using textile carbon fiber as the primary reinforcement in thin structural elements. These elements, characterized by their reduced-thickness concrete, demonstrate exceptional corrosion resistance and improved mechanical properties. Three specimens were analyzed experimentally and numerically, focusing on variations in fiber content. The flexural behavior was assessed regarding cracking load, ultimate load, crack propagation, and strain in the fiber strips. Doubling the fiber reinforcement resulted in a 35% increase in the maximum load capacity and enhanced rigidity. The experiment results were verified using a nonlinear finite element analysis (NLFEA), which was carried out with the assistance of the ANSYS software. There was only a 7.5% variance, which indicated that there was a high degree of concordance, as demonstrated by the findings. The fact that this is the case lends credence to the dependability of the model in the process of developing an ecologically friendly product.

Keywords: thin concrete slabs; fiber wraps; nominal flexural strength; numerical analysis.

Nomenclature

A_f	Area of the fiber, $mm^{2.}$
C.O.V	Coefficient of variance, %.
FRP	Fiber reinforcement polymer.
HRWR	High-range water reducer.
P	The load level applied in the flexure test, kN.
P_{cr}	The crack load at which the first crack appeared, kN.
P_u	The numerical ultimate load level, kN.
P_f	The experimental failure load level, kN.
Δ_{cr}	Deflection at mid-span under the crack load level, mm.
Δ_u	Deflection at mid-span under the ultimate load level, mm.
Δ_f	Deflection at mid-span under the failure load level, mm.

1. INTRODUCTION

The pressing demand for secure accommodations for individuals without homes, whether resulting from political strife or natural disasters, has emerged as a prominent issue. Additionally, there has been a growing inclination towards constructing more resilient marine and coastal infrastructure. Moreover, employing lighter construction materials can significantly enhance the lateral stability of buildings located in areas prone to strong seismic activity. Thin slabs reinforced with fiber textiles can serve as a viable substitute for traditional reinforced concrete in the building industry, offering advantages regarding engineering and environmental considerations. From an environmental standpoint, using elements with thinner thicknesses and a matrix of recycled supplementary cementitious materials instead of a portion of cement leads to a decrease in the overall production of concrete. As a result, lighter elements can be installed with fewer cement batches, reducing CO2 emissions. From an engineering perspective, using fiber with strong mechanical qualities and easy formability can create elements with high corrosion resistance and enhanced mechanical capabilities. This allows architects to realize more innovative concepts while adhering to a sustainable approach with green concrete. Plain concrete is the traditional construction material, but owing to its low resistance to tensile stresses, additives shall be used to enhance its mechanical behavior under different types of loading [1].

Fiber-reinforced concrete (FRC) is a type of concrete that contains traditional concrete ingredients along with randomly distributed short fibers. These fibers make up 0.3% to 2.5% of the volume of the concrete. The properties of the fibers, such as their type, shape, percentage, and aspect ratio (the fiber length ratio to diameter), determine the improvements in the mechanical properties of the concrete. The flexural strength of the material increases as the ratio of fibers increases. However, this also negatively affects the material's workability because the dispersed segments of fibers can clump together and hinder the mixing process. Therefore, the ratio of fibers must be adjusted to balance the mixture's strength and workability. As tested in [2], the results implied an improvement in compressive and flexural characteristics of 10% and 20%, respectively, in addition to failure mode transformation to ductile ones.

In the past ten years, there has been a growing interest in using fiber textiles as a primary reinforcement for cement components, combining the advantages of fiber-reinforced concrete and ordinary reinforced concrete and providing a more durable and sustainable structure with non-metallic textile reinforcement. The structures of TRC provide thinner structural elements due to their anti-corrosion behavior. Only a 3 mm cover was enough to avoid debonding failure and ensure full utilization of the anti-crack role of fibers [3]. Using lighter concrete elements and reducing the number of cement batches can significantly contribute to a cleaner environment and a more stable future temperature. The release of carbon dioxide (CO2), a greenhouse gas created during cement manufacture, is a crucial factor in environmental pollution and global warming [4]. A cradle-to-gate life cycle assessment (LCA) was conducted in [5] to compare the effectiveness of ordinary reinforced concrete versus carbon textile reinforced concrete based on available and transparent data. LCA studies the environmental aspect and potential impacts throughout a product's life, i.e., from cradle to gate, from raw material extraction through production, exploitation, and disposal or recycling. The study showed that TRC showed a comparatively improved effect in three impact categories: abiotic depletion of fossil resources (ADPF), acidification potential (AP), and global warming potential (GWP). TRC with carbon fiber mesh reinforcement was tested in [6]. The matrix was fine aggregate concrete made of sand. The experiment with mesh size as a main variable showed that a reduction of mesh size from 20 to 0 mm induced an effective role in flexure strength propagation. However, zero mesh size provided reversible results due to a lack of bond strength between the upper and lower layers of the matrix. Temperature-controlled and locally available components of normal-weight concrete were examined thoroughly by numerical and experimental investigation in this study regarding fiber reinforcement ratio, slab thickness, and matrix strength.

Following the prevailing inclination towards environmentally friendly concrete, waste materials are repurposed and employed as supplementary cementitious ingredients, such as fly ash and silica fume. In modern times, most concrete mixtures incorporate supplementary cementitious ingredients, which serve as a fraction of the binding agent in concrete. These supplementary materials can be derived from natural sources or produced through artificial methods. Pozzolans are materials that lack cementitious capabilities on their own. However, when combined with Portland cement and exposed to water, they undergo a reaction and create cementitious compounds. In conjunction with cement, these compounds serve as the binding elements in the concrete mixture. Supplementary cementitious materials, also known as mineral admixtures, must adhere to the standards set by existing regulations in each region. They can be used separately or in conjunction with concrete. They can be accompanied by the concrete mixture either as a binding element or as a distinct component that is batched separately at the ready-mixed concrete plant. Class F and class C fly ash can be utilized with a substitution dosage of 25-40% and 15-25%, respectively [7-8]. The presence of

silica fumes in the transition zone of concrete leads to a decrease in pores, even 12 and 24 hours early. This results in improved durability, increased splitting tensile strength, and enhanced flexural properties of concrete when the dose of silica fume is 15% or below [9-11]. Silica fume improved the performance of pozzolan-based cement concrete (NP) and ordinary Portland cement concrete (OPC). Adding 5% silica fume to the OPC and NP mix increased the compressive strength of the matrix compared to using NP alone. Using silica fume also reduced drying shrinkage and significantly enhanced the coefficient of chloride diffusion for OPC-NP and OPC-NP-SF, with improvements of 63% and 86%, respectively, [12]. In this study, a replacement dosage of 10% was used in one mix to take advantage of its effects.

Previously published studies on thin slabs and their applications were presented in this section. The experiment aimed to enhance the adhesion between textiles and mortar by applying sand of varying grain sizes to the textiles. The experiment included four different grain sizes of sand: no sand, 0.15-0.3 mm, 0.3-0.6 mm, and 0.6-1.20 mm. The test findings indicated that silica sand particles with a size range of 0.3-0.6 mm exhibit superior control over flexure, bond strength, and deformed shape compared to other specified sizes mentioned in [13]. The study examined ten U-shaped specimens that had metallic and nonmetallic reinforcement mesh and tension and compression bar reinforcement [14]. The specimens were divided into five series. Series A served as the control group without any meshes. Series B had layers of expanded steel mesh; Series C had layers of welded steel mesh; Series D had glass fiber mesh; and Series E was similar to B but without steel bars or increased steel bars in tension. The composition of the mortar matrix was specifically formulated to attain a compressive strength of 350 kg/cm2 after 28 days. This composition consists solely of fine particles and excludes coarse material. A four-point loading test was conducted to compare the mechanical properties of the five series. The use of welded galvanized steel mesh resulted in greater values for the first crack load, ultimate load, and energy absorption. However, it exhibited a worse ductility ratio (Δ at failure/Δ at yield) than specimens reinforced with glass mesh. Incorporating polypropylene fibers in the mixture enhanced first crack load, peak load, toughness, and reduced deflection for equivalent load levels. Utilizing multiple reinforcement meshes improved the initial cracking load, maximum load, and energy absorption.

The precast cold-formed steel ferrocement composite slab system was investigated in [15]. Increasing the slab thickness didn't affect load capacity prominently but delayed the formation of cracks at an early stage. Decreasing the spacing between studs to 150 mm resulted in an increase in load capacity by almost one-third. Uniaxial tensile strength was determined for 28 groups of textile-reinforced mortar specimens to study the effect of the textile layers and dispersed short fiber content in the mortar matrix [16]. The thermo-mechanical behavior of two TRC composites was studied at a macro-scale level under an axial tensile load, and textile-reinforced specimens showed an improvement in thermomechanical characteristics by increasing the number of phases on the stress-strain curve [17].

Glass fiber textiles can be used in retrofitting existing RC works, such as blast mitigation. The efficiency of the retrofitting system is measured by displacement and damage reduction. Two layers of chopped-strand glass mat (2LCSM) showed prominent behavior in limiting damage and forbidding fragments of the building [18-19]. The numerical study was performed on the capability of carbon fiber textiles (CFT) to strengthen simple slabs under impact loads using the finite element method [20]. Carbon fiber textiles limited the peak and residual displacement for thin elements, but for thicker ones, its effect was limited as punching was the dominant factor. The experimental results in this inquiry were validated using ANSYS software, enabling the utilization of reliable models for the development of lightweight, high-strength, and environmentally friendly concrete slabs.

2.Test Program

2.1 Textiles Preparation

The experiment utilized SikaWrap®-230 C, a unidirectional woven carbon fiber product from Sika Corporation, as shown in Fig. 1. The carbon fiber was impregnated with Sikadur®-330 adhesive material, serving as a resin, utilizing a manual hand layup process. Carbon fiber offers flexibility, resistance to corrosion, moderate stability at high temperatures, and low density. This product is classified as an anti-pollution and ecologically beneficial product according to Regulation (EC) No. 1907 [21]. The Sikadur®-330 resin comprises two components, labeled A and B, mixed in a ratio of 4 to 1, respectively, based on weight. Components A and B were thoroughly combined individually before being mixed, resulting in a uniform and cohesive adhesive substance with a gray hue, as shown in Fig. 2. In the hand layup procedure, a smooth sponge roll was employed to effectively join the fibers together, as depicted in Fig. 3. Table 1 provides a concise overview of the mechanical characteristics of the fiber and resin. The mechanical qualities of fiber strips and the technique of mixing the adhesive substance adhere to the specifications outlined in the datasheet provided by a reputable manufacturer with a long-standing presence in the local market.

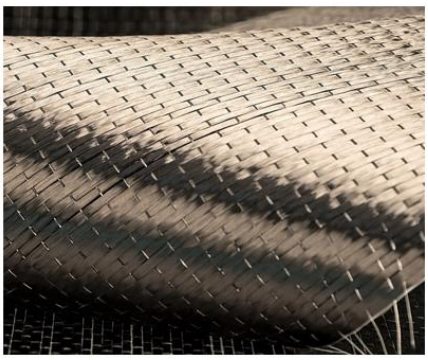

Fig 1: Sika Wrap®-230 c unidirectional woven carbon fiber.

Fig 2: Mixing process of component B with component A, forming the resin matrix Sikadur®-330.

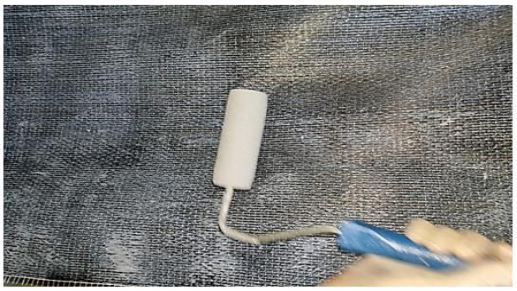

Fig 3: Impregnation by Sikadur®-330 as a resin using the manual hand layup method.

Table 1: The mechanical properties of fiber-reinforced polymer components.

Type	Density g/cm^3	Tensile strength N/mm^2	Modulus of elasticity kN/mm^2	Elongation %
Fiber SikaWrap-230C	1.82	3,200 (ASTM D 3039) [22]	210 (ASTM D 3039) [22]	1.59 (ASTM D 3039) [22]
Sikadur -330	1.3 ± 0.1	30 (7 days at +23 C) (ISO 527) [23]	3.8 (7 days at +23 C) (ISO 527) [23]	0.9 (7 days at +23 C) (ISO 527) [23]

Table 2: The mix proportions of the concrete matrix.

Slump (mm)	C.O.V (%)	Density (kg/m3)	C.O.V (%)	Average cubic compressive strength (MPa)	C.O.V (%)	Average splitting tensile strength (MPa)	C.O.V (%)
87	4	2300	2.4	36.5	4.2	3.7	3.8

Table 3: The characteristics of fresh and hardened concrete.

Cement (Kg/m^3)	Water (Kg/m^3)	Coarse Agg. (Kg/m^3)	Fine Agg. (Kg/m^3)	S.F (Kg/m^3)	HRWR (Kg/m^3)
360	200	910	850	40	3

2.2Concrete Matrix

The study utilized a standard-weight concrete matrix, which is detailed in Table 2. The coarse and fine aggregate's maximum aggregate size was determined using a sieve analysis test, as shown in Fig. 4, and recorded as 12.50 mm and 2.36 mm, respectively, per ASTM [22]. Additionally, a high-range water reducer (Master Glenuim RMC 315) was included in the mixture at a ratio of 0.75% of the total binder

An assessment was conducted on the workability of fresh concrete by measuring its slump value. Additionally, the characteristics of hardened concrete were determined. To specify the compressive strength and density, six cubes with dimensions of 100 x 100 x 100 mm were prepared. Furthermore, three cylinders

Fig 4: Sieve analysis test for coarse and fine aggregate

were prepared to determine the tensile characteristics using an indirect tensile strength test. All tests were conducted following BS EN 206 [24]. The test results are summarized in Table 3.

2.3Test Specimens

This work aims to study the flexural performance of slabs reinforced by adhesive-impregnated fiber textile strips. Three one-way concrete slab strips were investigated; a three-point loading test was employed to study this type of concrete slab rather than a four-point loading; one-way concrete slab strips were provided parallel to the direction of loading; and a strain gauge was attached to the middle strips to measure the strain of fiber at different loading levels, as shown in Fig. 5. This investigation was performed to study the structural behavior of slabs under static loads regarding textile reinforcement content in tension, as shown in Fig. 6.

Fig 5: Strain gauges were attached to the carbon fiber textiles.

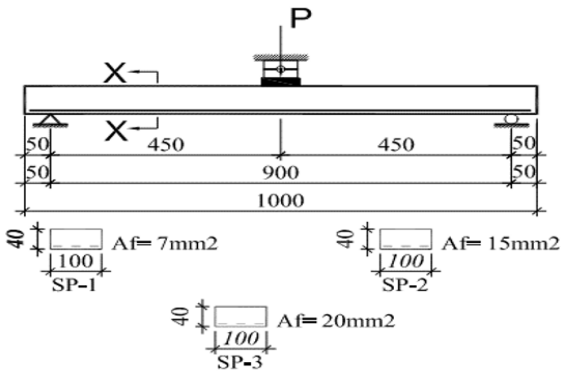

Fig **6:** Layout and detailed sections of the tested slabs.

2.4 Specimens Preparation

The wooden forms were coated with oil to prevent the wood from absorbing water and to make it easier to remove the forms once the specimen had hardened. The concrete was then poured into the mold to a suitable depth, ensuring that there was a 5 mm layer of concrete covering the FRP strips. The strain gauge was placed on the middle strip, as depicted in Fig. 7. For the initial 24-hour period, the specimens were stored beneath a vapor barrier to preserve their moisture. Subsequently, the specimens were placed in a water basin with a consistent ambient temperature of 25 ± 2 C° for curing. After 7 days, three cubes were extracted from each variant of concrete to conduct a compressive strength test. The remaining specimens were extracted and subjected to testing when they reached the age of 28 days. Wooden forms were oiled to prevent water absorption by the wood and facilitate form removal after specimen hardening. Concrete was cast in the mold to an appropriate depth, providing a 5 mm concrete cover for FRP strips. The middle strip is accompanied by the strain gauge, as shown in Fig. 7. During the first 24 hours, specimens were kept below a vapor barrier to maintain their humidity; afterward, specimens were cured in a water basin with an ambient temperature of 25 ± 2 C°. After 7 days, three cubes from each type of concrete were removed for the 7-day compressive strength test. The rest of the specimens were removed and tested at the age of 28 days.

Fig 7: Stages of the specimen's preparation

2.5 Specimens Test Setup

The slab strips underwent testing using a three-point loading machine with a maximum capacity of 100 kN. The load was delivered in the center of the span using a properly sized cylinder to prevent local bearing failure, as depicted in Fig. 8. Strain gauges have been adhered to carbon fiber strips in the middle section to quantify the strain values of FRP strips under various levels of loading. The deflection of slabs at various loading levels was measured using two LVDTs. The LVDTs were positioned 300 mm apart. However, due to limitations with the testing machine, it was not possible to fix an LVDT at the mid-span. Consequently, the values at the mid-span were determined by interpolating between the two measured values using simple equations integrated by the double integration method. To determine the failure mechanism and fracture propagation, crack patterns were marked on the lower surface of the slabs throughout each loading step until failure occurred.

Table 4: Properties of the tested slabs.

Specimen	Slab thickness (mm)	Provided mesh area A_f (mm^2)	Fiber V_f (%)
SP-1	40	7	0.18
SP-2	40	15	0.38
SP-3	40	20	0.50

Fig 8: Test setup for the tested slabs.

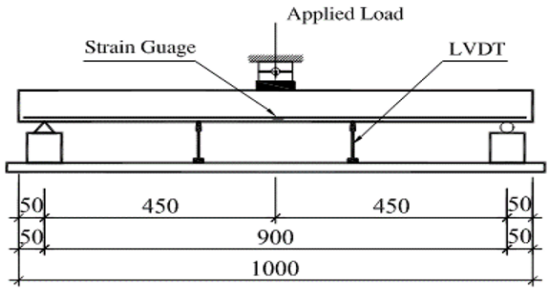

Fig 9: Schematic elevation for loading test setup

3.Experimental Results and Discussion

3.1Crack Load P_{cr}

It can be implied from the results in Table 5 that the fiber content can't be explicitly considered as a parameter of the crack load initiation process as the specimens recorded somehow the same cracking load. They recorded a cracking load of around 0.38 kN with a standard deviation of 0.03 and a coefficient of variance equal to 7.96%.

Table 5: Detailed experimental and numerical results for twelve specimens subjected to flexure with three main variables regarding load, deflection, stiffness, and section. The curves and energy absorption

Slab Symbol	Experimental results				Numerical results			
	P_{cr}	Δ_{cr}	P_u	Δ_u	P_{cr}	Δ_{cr}	P_u	Δ_u
	kN	*mm*	*kN*	*mm*	*kN*	*mm*	*kN*	*mm*
SP-1	0.35	0.60	2.42	38.61	0.39	0.46	2.68	35.57
SP-2	0.41	0.68	3.17	31.64	0.39	0.46	2.92	28.63
SP-3	0.39	0.61	3.81	26.29	0.41	0.52	4.02	25.80

3.2 Load-Deflection Curves

The deflection at the midpoint was plotted on the horizontal axis, while different load levels were plotted on the vertical axis for each specimen, as depicted in Fig. 10. The specimens exhibited a linear behavior until the first crack appeared, at which point the displacement abruptly increased under a narrow range of loads due to the reduction in stiffness of the cracked section. The curves show that an increase in the fiber reinforcement content leads to an improvement in the flexure capacity and stiffness rigidity of specimens due to magnifying the exploitation of tensile and compressive resisting areas for the slab sections. For instance: an increase in fiber content for SP-2 and SP-3 compared to SP-1 by 111% and 177.7%, respectively, an increase in ultimate load of 31.0% and 57.44%, respectively, and a reduction in deflection values at the failure load level of SP-1 as a datum by 41% and 72.21%, respectively. The ultimate load comparisons were presented graphically in Fig. 11.

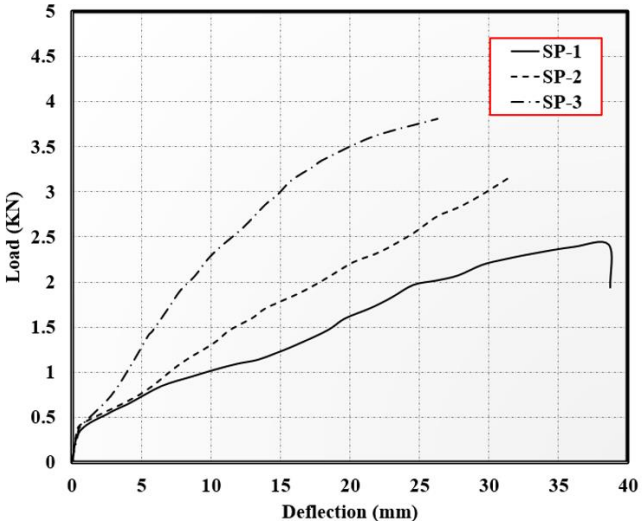

Fig 10: Load-deflection curves of specimens SP-1, SP-2, and SP-3

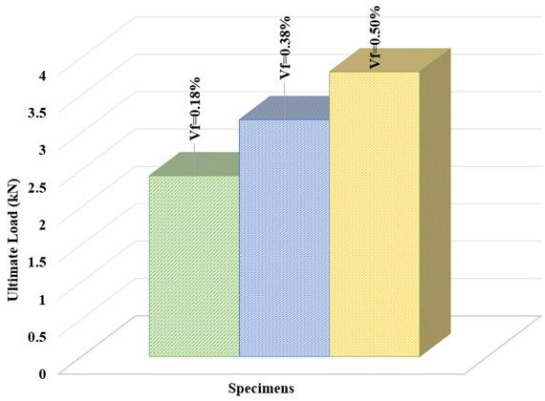

Fig 11: Graphical comparison between specimens' ultimate load results.

3.3Strain in Fiber Strips

Strain gauges were attached to the fiber strips to measure the strain in the fiber at different load levels; the load level was presented by the vertical axis, and strain values were given by the horizontal axis. Generally, strain followed the same behavior of deflection under different load levels regarding the variables investigated in this work, as presented in Fig. 12. Specimens SP-2 and SP-3 showed a reduction in the strain at the failure load level of SP-1 as a control by 38.92% and 56.82%, respectively.

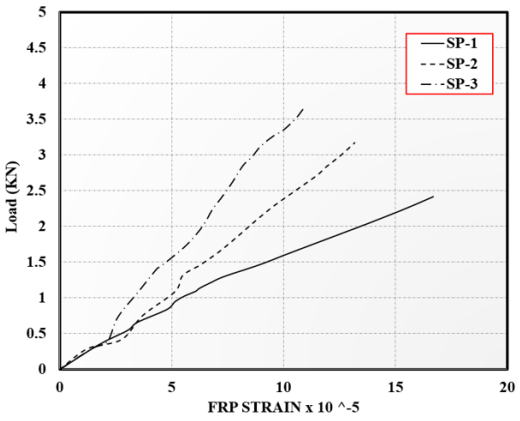

Fig 12: Load-FRP strain curves of specimens SP-1, SP-2, and SP-3.

3.4 Failure modes and crack patterns

The fracture patterns and failure modes of each specimen were determined by marking the propagation of cracks at the lower edge of each slab. Typically, the initial fracture occurs in the mid-span with high stress, indicating that plain concrete has low resistance to tensile stresses. When the compressive stresses exceed the crushing capacity of the concrete, crack breadth increases, and the pattern spreads quickly along the lower fiber at higher load levels. Additionally, significant compressive stresses arise at the top edge of the plain matrix. As a result, failure happens immediately. The failure is caused by the crushing of concrete, which is a result of the fiber strips having a high resistance to tension. This resistance prevents the fibers from suddenly rupturing. The diagram illustrating the stages of crack development leading to failure can be seen in Fig. 13. Figure 14 displays the crack patterns observed in each specimen. To mitigate the risk of abrupt brittle failure in concrete, particularly when using high-strength materials such as carbon fiber, a greater factor of safety is employed in the design of these thin elements.

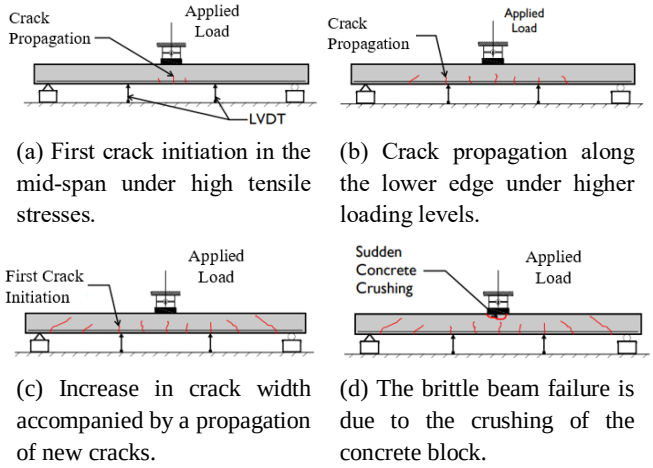

(a) First crack initiation in the mid-span under high tensile stresses.

(b) Crack propagation along the lower edge under higher loading levels.

(c) Increase in crack width accompanied by a propagation of new cracks.

(d) The brittle beam failure is due to the crushing of the concrete block.

Figure 13: Schematic illustration for crack propagation until failure.

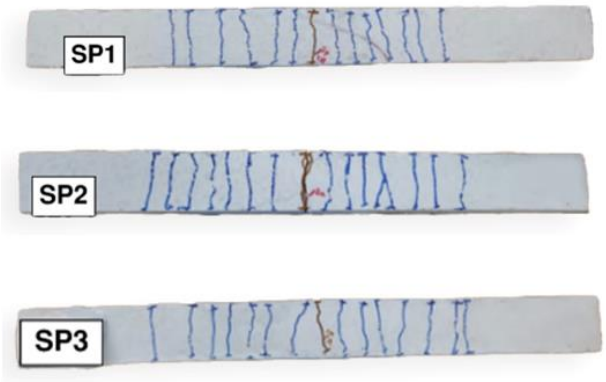

Fig 14 Crack patterns for the tested specimens.

4.Numerical Analysis

4.1Nonlinear Finite Element Analysis

Finite element analysis (FEA) is an essential tool in the research field, allowing researchers to investigate the linear and nonlinear behavior of various structures subjected to different types of loads. Experimental studies that require less time and are less expensive can be simulated using Finite Element Method (FEM) software programs, which can vary parameters. In this inquiry, ANSYS V15.0 [25] was used to validate the experimental studies through numerical models. The SOLID 65 element type is chosen to model the concrete matrix. This element type allows for the definition of compressive and tensile properties under various loading conditions, enabling the formation of cracks in tension and compression zones once the strength limit is surpassed. The longitudinal fiber strips were simulated using the LINK180 element type, following a linear stress-strain curve provided by the manufacturer.

4.2Experimental Results Validation with Nonlinear Finite Element Analysis Models

The ANSYS models were used to validate the experimental results for each specimen, as depicted in Fig. 15. Load-displacement curves were obtained from the data, as shown in Fig. 16. The crack propagation and failure modes exhibited identical behavior to that observed in the experimental work. Initially, a fracture emerged at the mid-span of the beam, followed by the propagation of cracks along the beam under increased loads. Ultimately, the slab failed due to the crushing of the concrete zone.

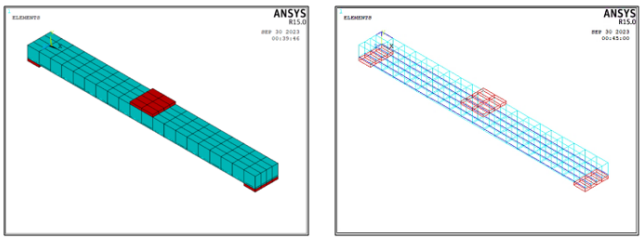

Fig 15: Typical model for the numerical analysis

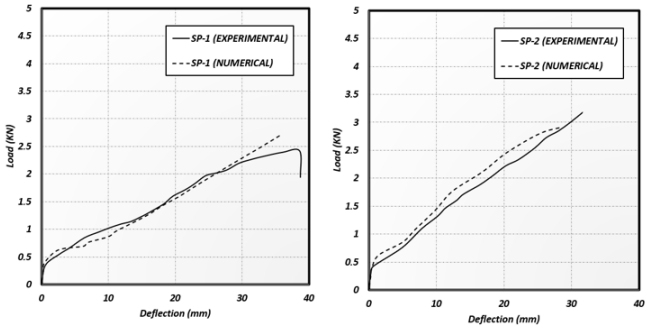

Fig 16**:** Comparison between experimental and numerical results.

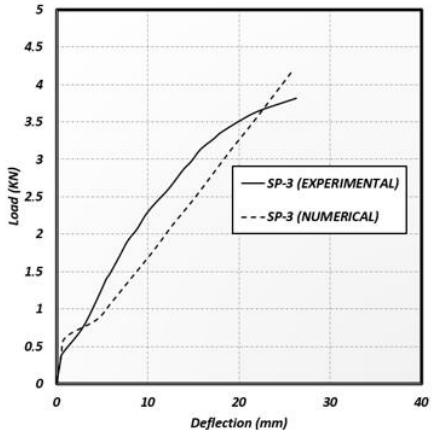

Cont. Fig 16**:** Comparison between experimental and numerical results

.

The numerical results for all slabs showed high reconciliation with the experimental results, comparing the recorded results in Table 5. It can be exhibited that the overall ultimate load average ratio ($P_{u\ exp.}/P_{u\ num}$) is 0.95 and the overall deflection at failure ratio ($\Delta_{u\ exp.}/\Delta_{u\ num}$) is 1.07.

5.Conclusion

The flexural behavior of thin concrete slabs reinforced with textile carbon fiber, renovated for the urgent need for less pollutant, more durable, and lighter-weight concrete elements, was investigated using experimental and numerical analysis, and the following conclusions can be drawn:

1. Fiber-textile reinforcement improves the flexural behavior of the thin slabs; it enhances the ultimate load by around 45% for a 140% increase in reinforcing content, but it's not a permanent, directly proportional relationship. Bond strength plays a vital role in higher reinforcing ratios.
2. FRP strain values were measured, and the recorded results imply that there was no failure due to slippage of FRP textiles.
3. The failure is caused by the crushing of concrete, which is a result of the fiber strips having a high resistance to tension. This resistance prevents the fibers from suddenly rupturing.
4. The numerical analysis corroborated the experimental findings. However, it is recommended that future studies focus on the bond strength to ensure comprehensive understanding and validation.

References

[1] M. Słowik, "The analysis of failure in concrete and reinforced concrete beams with different reinforcement ratios," *Archive of Applied Mechanics*, vol. 89, pp. 885–895, 2019.

[2] F. Shi, T. M. Pham, H. Hao, and Y. Hao, "Post-cracking behavior of basalt and macro polypropylene hybrid fiber reinforced concrete with different compressive strengths," *Contortion and Building Materials*, vol. 262, p. 120108, 2020, doi: https://doi.org/10.1016/j.conbuildmat.2020.120108.

[3] S. Yin, S. Xu, and H. Li, "Improved mechanical properties of textile-reinforced concrete thin plate," *Journal of the Wuhan University of Technology-Mater. Sci. Ed.*, vol. 28, no. 1, pp. 92–98, 2013, doi: 10.1007/s11595-013-0647-z.

[4] D. Friese, M. Scheurer, L. Hahn, T. Gries, and C. Cherif, "Textile reinforcement structures for concrete construction applications; a review," *J Compos Mater*, vol. 56, no. 26, pp. 4041–4064, 2022.

[5] N. Stoiber, M. Hammerl, and B. Kromoser, "Cradle-to-gate life cycle assessment of CFRP reinforcement for concrete structures: calculation basis and exemplary application," *J Clean Prod*, vol. 280, p. 124300, 2021.

[6] M. Halvaei, M. Jamshidi, M. Latifi, and M. Ejtemaei, "Experimental investigation and modeling of flexural properties of carbon textile-reinforced concrete," *Construction Building Materials*, vol. 262, p. 120877, 2020, doi: https://doi.org/10.1016/j.conbuildmat.2020.120877.

[7] M. Ahmaruzzaman, "A review on the utilization of fly ash," *Prog Energy Combust Sci*, vol. 36, no. 3, pp. 327–363, 2010, doi: https://doi.org/10.1016/j.pecs.2009.11.003.

[8] C. Marthong and T. P. Agrawal, "Effect of fly ash additive on concrete properties," *Int J Eng Res Appl*, vol. 2, no. 4, pp. 1986–1991, 2012.

[9] R. Siddique, "Utilization of silica fume in concrete: Review of hardened properties," *Resour Conserv Recycl*, vol. 55, no. 11, pp. 923–932, 2011, doi: https://doi.org/10.1016/j.resconrec.2011.06.012.
[10] A. Behnood and H. Ziari, "Effects of silica fume addition and water-to-cement ratio on the properties of high-strength concrete after exposure to high temperatures," *Cement Concrete Composites*, vol. 30, no. 2, pp. 106–112, 2008.
[11] M. Mazloom, A. A. Ramezanianpour, and J. J. Brooks, "Effect of silica fume on mechanical properties of high-strength concrete," *Cement Concrete Composites*, vol. 26, no. 4, pp. 347–357, 2004, doi: https://doi.org/10.1016/S0958-9465(03)00017-9.
[12] S. Ahmad, O. S. B. Al-Amoudi, S. M. S. Khan, and M. Maslehuddin, "Effect of silica fume inclusion on the strength, shrinkage, and durability characteristics of natural pozzolan-based cement concrete," *Case Studies in Construction Materials*, vol. 17, p. e01255, 2022.
[13] Q. Li and S. Xu, "Experimental research on the mechanical performance of hybrid fiber-reinforced cementitious composites with polyvinyl alcohol short fiber and carbon textile," *J Compos Mater*, vol. 45, no. 1, pp. 5–28, 2011.
[14] Y. B. I. Shaheen and E. A. Eltehawy, "Structural behavior of ferrocement channel slabs for low-cost housing," *Challenge Journal of Concrete Research Letters*, vol. 8, no. 2, pp. 48–64, 2017.
[15] M. Abu Hamed, S. Y. Mahfouz, and A. E. Zakaria, "Bending behavior of composite ferrocement slabs in cold-formed steel floors, *Faculty of Engineering, Cairo University Journal*, 2018".
[16] Z. Dong, M. Deng, C. Zhang, Y. Zhang, and H. Sun, "Tensile behavior of glass textile reinforced mortar (TRM) added with short PVA fibers," *Construction and Building Materials*, vol. 260, p. 119897, 2020, doi: https://doi.org/10.1016/j.conbuildmat.2020.119897.
[17] T. H. Nguyen, X. H. Vu, A. Si Larbi, and E. Ferrier, "Experimental study of the effect of simultaneous mechanical and high-temperature loadings on the behavior of textile-reinforced concrete (TRC)," *Construction and Building Materials*, vol. 125, pp. 253–270, 2016, doi: https://doi.org/10.1016/j.conbuildmat.2016.08.026.
[18] H. Draganić, G. Gazić, S. Lukić, and M. Jeleč, "Experimental investigation on blast load resistance of reinforced concrete slabs retrofitted with epoxy resin impregnated glass fiber textiles," *Compos Struct*, vol. 274, p. 114349, 2021, doi: https://doi.org/10.1016/j.compstruct.2021.114349.
[19] Z. Dong, M. Deng, J. Dai, and S. Song, "Flexural strengthening of RC slabs using textile reinforced mortar improved with short PVA fibers," *Construction and Building Materials*, vol. 304, p. 124613, 2021, doi: https://doi.org/10.1016/j.conbuildmat.2021.124613.
[20] B. Batarlar and S. Saatci, "Numerical investigation on the behavior of reinforced concrete slabs strengthened with carbon fiber textile reinforcement under impact loads," *Structures*, vol. 41, pp. 1164–1177, 2022, doi: https://doi.org/10.1016/j.istruc.2022.05.057.
[21] Euro Code (EC) No. 1907: Registration, Evaluation, Authorization, and Restriction of Chemicals (REACH), 2006.
[22] American Society for Testing and Materials (ASTM), C496/C496M-17, C873/C873M-23, and C143/C143M-20, 2020.
[23] International Organization for Standardization (ISO 527), Plastics Determination of tensile properties, Part 4, 2023.
[24] British Standards (BS EN 206), EN 12350-4, EN 12390-3, and EN 1239-6, 2021.
[25] ANSYS-Release Version 15.0, A Finite Element Computer Software and User Manual for Nonlinear Structural Analysis, ANSYS Inc., Canonsburg, PA, 2013.